RSC Advances

PAPER

Cite this: *RSC Adv.*, 2023, **13**, 30925

A novel portable immuno-device for the recognition of lymphatic vessel endothelial hyaluronan receptor-1 biomarker using GQD–AgNPrs conductive ink stabilized on the surface of cellulose†

Ahmad Mobed, ‡[abc] Fereshteh Kohansal,‡[d] Sanam Dolati *[c] and Mohammad Hasanzadeh *[ad]

Lymphatic vessel endothelium expresses various lymphatic marker molecules. LYVE-1, the lymphatic vessel endothelial hyaluronan (HA) receptor, a 322-residue protein belonging to the integral membrane glycoproteins which is found on lymph vessel wall and is completely absent from blood vessels. LYVE-1 is very effective in the passage of lymphocytes and tumor cells into the lymphatics. As regards cancer metastasis, *in vitro* studies indicate LYVE-1 to be involved in tumor cell adhesion. Researches show that, in neoplastic tissue, LYVE-1 is limited to the lymphovascular and could well be proper for studies of tumor lymphangiogenesis. So, the monitoring of LYVE-1 level in human biofluids has provided a valuable approach for research into tumor lymphangiogenesis. For the first time, an innovative paper-based electrochemical immune-platform was developed for recognition of LYVE-1. For this purpose, graphene quantum dots decorated silver nanoparticles nano-ink was synthesized and designed directly by writing pen-on paper technology on the surface of photographic paper. This nano-ink has a great surface area for biomarker immobilization. The prepared paper-based biosensor was so small and cheap and also has high stability and sensitivity. For the first time, biotinylated antibody of biomarker (LYVE-1) was immobilized on the surface of working electrode and utilized for the monitoring of specific antigen by simple immune-assay strategy. The designed biosensor showed two separated linear ranges in the range of 20–320 pg ml^{-1} and 0.625–10 pg ml^{-1}, with the acceptable limit of detection (LOD) of 0.312 pg ml^{-1}. Additionally, engineered immunosensor revealed excellent selectivity that promises its use in complex biological samples and assistance for biomarker-related disease screening in clinical studies.

Received 4th September 2023
Accepted 16th October 2023

DOI: 10.1039/d3ra06025j

rsc.li/rsc-advances

1. Introduction

Cancer is among the most critical health issues worldwide.[1] Treatment of cancer poses considerable difficulties such as resistance to multiple drugs and a scarcity of therapies that target tumors specifically while causing minimal adverse effects.[2] Recent advances in cancer immunotherapy have focused on enhancing the body's natural antitumor immune response. This can be achieved through various approaches, such as checkpoint inhibitors, which block proteins that inhibit immune responses, adoptive T cell therapy[3–5] and peptide-based therapy[2,6,7] which is new strategy in cancer treatment. The predominant mode of metastasis in cancer cells is through the blood and lymphatic vessels, resulting in the colonization of distant organs and lymph nodes, which ultimately leads to unfavorable prognosis. Consequently, curtailing the dissemination of cancer cells through the blood and lymphatic systems has been a central area of interest in cancer research for many years.[8]

Lymphatic vessels have an important role in maintaining tissue-fluid homeostasis, immune surveillance and metastasis.[9] LYVE-1 is a receptor for hyaluronan and has been known as a potent marker for lymphatic endothelium.[10] It is structurally related to CD44 and other HA-binding proteins. The most significant feature of LYVE-1 is its pattern of tissue expression.[11] LYVE-1 is selectively expressed in the endothelia of lymphatic capillaries and also expressed in spleen endothelium, alveolar

[a]*Pharmaceutical Analysis Research Center, Tabriz University of Medical Sciences, Tabriz 51664, Iran. E-mail: hasanzadehm@tbzmed.ac.ir*

[b]*Aging Research Institute, Faculty of Medicine, Tabriz University of Medical Sciences, Iran*

[c]*Physical Medicine and Rehabilitation Research Center, Aging Research Institute, Faculty of Medicine, Tabriz University of Medical Sciences, Iran. E-mail: sanam.dolati@gmail.com*

[d]*Nutrition Research Center, Tabriz University of Medical Sciences, Tabriz, Iran*

† Electronic supplementary information (ESI) available. See DOI: https://doi.org/10.1039/d3ra06025j

‡ Equal contribution.

lining epithelium, liver sinusoidal endothelial cells (LSEC), and activated tissue macrophages.[12,13] On the other hand, LYVE-1 is a promising diagnostic and prognostic biomarker in several types of cancer including gastric, lung, liver, pancreas, and breast cancer.[14–17] LYVE-1 is likely to play a role in either hyaluronan homeostasis or in the regulation of cellular trafficking to the lymph nodes.[18] The lymphatics are an important route for early metastasis in cancer. The LYVE-1 has been extensively used for the detection of tumor-associated lymphatic vessels in different types of tumors.[19] During cancer progression, expression of LYVE-1 is increased in lymphatic endothelial cells. A high density of lymph vessels expressing LYVE-1 is associated with a high frequency of regional lymph node metastases.[20] Immunohistochemical intensity of LYVE-1 expression is beneficial for monitoring of lymphatic invasion or lymphangiogenesis in different kinds of cancers, such as gastric, pulmonary, colon, mammary, endometrial/testicular cancers, and neuroblastomas/vascular tumors.[21,22]

The detection of LYVE-1 as a precise biomarker for lymphatic vasculature provides a possible minimally-invasive method for predicting disease progress.[23] The detection and quantification of LYVE-1 can provide important information valuable for clinical cancer diagnosis. There are various approaches for detection of the LYVE-1 molecule as an integral membrane glycoprotein, such as immunofluorescence microscopy, flow cytometry and immunohistochemistry.[24,25] During the last decade, a growing number of scientists have focused on developing rapid techniques. However, the growing sensitivity of detection methods poses a challenge in differentiating between insignificant alterations and lesions that have the potential to progress to malignant cancer.[26]

Biosensors as excellent tools in medical analysis allows accurate detection of biomarkers of diseases. Biosensors are efficient tools for the rapid, qualitative and quantitative measurement of biomarkers in animal/human biofluids.[27,28] Biosensors with sensitive and specific features could give advantage to the progress of LYVE-1 detection platforms. The results of this investigation contribute to the detection of LYVE-1 by biosensing system.

Immunosensors are commonly employed across various domains due to their exceptional sensitivity. However, the utilization of these biosensors necessitates multiple stages of preparation, skilled technicians, and expensive equipment.[29] In order to address this issue, paper-based immunoassays have been developed and are being explored by numerous researchers.[30] Paper, owing to its advantageous properties, emerges as a highly favorable material for this purpose.[31] It boasts attributes such as ease of manipulation, absence of the need for specialized tools, reusability, cost-effectiveness, and a hydrophilic platform that allows the passage of liquid substances without the requirement for external power sources.[30] Consequently, paper plays a pivotal role in the fabrication of paper-based immunosensors, serving as a substantial and economical substrate for the immobilization of reagents and their subsequent reactions. The fibrous and porous structure inherent to paper offers significant advantages for immobilizing reagents and facilitating their reactions. Capitalizing on capillary forces, paper efficiently directs aqueous liquid streams, providing an extensive surface area for reagent immobilization and a substantial region for ensuing reagent reactions.[32]

Recently, the practice of creating conductive patterns on paper has emerged as a cost-effective and straightforward method for crafting paper-based sensors.[33] This approach facilitates the economical and expedient production of customized electrodes. Consequently, paper-based sensors represent an attractive alternative to conventional electrochemical biosensors.[34] Given the critical demand within healthcare facilities such as clinical laboratories and medical research centers for the early detection of cancer, there exists a compelling need for these novel biosensors employing nano-inks. Nano-inks play a pivotal role in enhancing the efficiency of electrochemical immunosensors, enabling the rapid and facile detection of cancer.[35] For example, a paper-based genosensor by immobilization of ssDNA on the surface of AgNPs with graphene quantum was fabricated for detection of microorganism.[36,37] Also, a flexible label-free electrochemical biosensor was developed for the screening of miRNA-21 using Ag@Au/GQD core–shell as nano-ink stabilized on the surface of photographic paper.[37,38] Created novel platform was low-cost and performed as a paper-based laboratory technology.[39] Similarly, a flexible paper based electrochemical biosensor as a moveable device was advanced for recognition of ractopamine in animal feed. Planned biosensor was cost-effective and applicable for food quality control and analysis.[40] This study's outcomes offer novel insights into detection of LYVE-1 in complex samples, by using biosensor technology.

For the first time, novel conductive nano-ink based on GQDs–silver nanoprisms (GQDs–AgNPrs) was synthesized and used to preparation of three-electrode template on the surface of photographic paper by pen-on-paper technology. Due to quantum imprisonment and boundary effects due to changes in electronic distribution, and exhibit a bandgap responsible for their photoluminescence properties and changes in conductivity, which can be adjusted depending on the size and structure of the GQD.[41,42] GQDs have also been positively used in electrochemical sensors, which utilize redox reactions and other charge transfer phenomena to detect and quantify target analytes.[43] GQDs application in electrochemistry is also popular due to their ease of manufacture and the ability to be doped or modified for specific sensing requests.[44,45] These features enable GQD-based nanomaterials to have higher sensitivity and lower detection limits. In several cases, GQD can also be combined with other materials to create GQD-based nanocomposites with the purpose of creating a synergistic effect that facilitates the catalytic reaction with the target analyte.[45,46] QDs in some cases consider as a toxic material but the adverse effects caused by the first generations of QDs will likely be reduced by newer generations of QDs. The search for new nanoparticles that are as effective as current QDs but without proven toxic elements has been intensified, and very promising new luminescent NPs have been discovered in recent years.[47,48] Recently, luminescent carbon nanodots (C-dots), GQDs, and nanometer-sized graphene flakes with excellent optical and electronic

properties have been discovered recently. These NPs are very promising due to their chemical inertness, high specific surface area, and good surface grafting ability. Primary discoveries indicate that C-dots and GQD exhibit minimal cytotoxicity for exposed cells.[47,48]

Silver nanoparticles (AgNPs) exhibit exceptional properties and high electrical conductivity which making them a key component in enhancing the performance of conductive inks compared to other metal nanoparticles. The advantages of silver include outstanding electrical, optical, thermal characteristics, biocompatibility, low toxicity, and support for electrocatalytic activity.[49] However, the challenge arises from the tendency of AgNPs to aggregate and the subsequent solvent evaporation, which can lead to gaps in printed patterns and reduced conductivity.[50] Consequently, there is a pressing need to develop novel types of conductive ink.[33,49]

To address this issue, hybrid inks have been formulated by combining AgNPs with carbon based nanoparticles, as these compounds can effectively bridge the gaps between aggregated AgNPs, creating efficient electrical pathways.[50] Within this context, graphene quantum dots (GQDs) have gained prominence as zero-dimensional graphene nanocrystals, finding applications in optical[51] and electrochemical sensors,[52] lithium-ion batteries,[53] and bio-imaging.[54] These nanoparticles are exceptionally small, measuring just a few nanometers, and possess strong quantum confinement effects along with various functional groups.[49,55] Importantly, studies have revealed that the electronic properties of GQDs undergo significant changes as a result of their functionalization.

For the first time, the engineered interface utilized for the construction of novel paper-based immunosensor using immobilization of antibody on the working electrode zone of three-electrode system. So, based on immune-complex of antibody–antigen, the target biomolecule (LYVE-1) was identified by using electrochemical techniques. Interestingly a novel and powerful portable bioassay was proposed for the monitoring of LYVE-1 in human plasma samples, which promises its application in early-stage diagnosis of cancer.

2. Methods and materials

The ELISA kit containing antibody and antigen receptor, and dilution solution were purchased from ZellBio Co., Germany, polyvinylpyrrolidone K-30 (PVP) (molecular weight ≈ 300 g), graphite powder, chitosan, acetic acid, graphene quantum dots (GQD), ethanol, ethylene glycol, silver nitrate, sodium hydroxide, trisodiumcitrate (TSC), hydrogen peroxide, sodium borohydride ($NaBH_4$), potassium ferricyanide $K_3Fe(CN)_6$ and potassium ferrocyanide $K_4Fe(CN)_6$ were purchased from Sigma Aldrich (Ontario, Canada). Also, potassium chloride (KCl), *N*-hydroxysuccinimide (NHS), bovine serum albumin (BSA), and 1-ethyl-3-(3-dimethylaminopropyl)carbodiimide (EDC) were obtained from Merck KGaA, Germany. Humana plasma samples were gotten from the Iranian Blood Transfusion Center (Tabriz, Iran).

To begin, a PVP solution containing 0.06 g of PVP in 3 ml of water, was introduced into 200 ml of deionized water (DW). Then, a solution of $AgNO_3$ with a concentration of 0.01 M and a volume of 4 ml was added and mixed vigorously. Following that, a solution of TSC with a concentration of 75 mM and a volume of 8 ml was added to the mixture. Subsequently, 1 l of hydrogen peroxide was added and stirred. Afterward, a solution of $NaBH_4$ with a concentration of 100 mM and a volume of 3.2 l was introduced into the mixture. The inclusion of $NaBH_4$ as a reducing agent led to the formation of small AgNPrs, resulting in a highly intense yellow coloration of the solution. Within a few seconds, the color of the colloidal solution transitioned to a light-yellow shade. The resultant liquid was stirred at room temperature for 30 minutes, causing the hue to change to blue. The resulting colloidal mixture was then stored at a temperature of 4 °C for future utilization. To do this, 2 ml of 0.1 M acetic acid was used to dissolve 0.0113 g of chitosan before being sonicated. Chitosan was fully dissolved in the acid before being combined with 0.6 g of graphite and 0.2 g of PVP using a magnetic stirrer. 2 ml of pre-prepared GQDs were then added and given time to dissolve entirely. After that, 600 μl of silver nanoparticles were added. It is recommended to formerly set the oven to 60 °C. The resultant solution has to be incubated for 12 to 18 hours with its container completely sealed at 60 °C. Following this step, the solution remained for 3 minutes at 80 °C. The magnetic stirrer was deactivated after 3 minutes and a shaker or stirrer was switched on instead. Then, 0.12 g of sodium hydroxide dissolved in 400 μl of deionized water and added to the mixture, it was blended for three minutes using a magnetic stirrer. Finally, the mixture was washed three times with DW and alcohol for purification and utilization of electrodes preparation. Scheme 1 shows all of preparation steps of AgNPrs–GQDs conductive nano-ink.

The PalmSens 4c system was employed to carry out electrochemical measurements, and it was operated using the PSTrace software on a laptop. The measurements for chronoamperometry were taken with a 2 second equilibrium time and a voltage amplitude of 10 millivolts. AgNPrs–GQDs nano-ink was utilized to create paper electrodes, which were employed as a working electrode, a reference electrode, and a counter electrode. It is worth mentioning that, we synthesized and prepared the AgNPrs–GQDs nano-ink, then utilized a high-resolution field emission scanning electron microscope (FE-SEM) called Hitachi SU8020 from Czech to examine the morphology of the electrode surface. Additionally, we used energy dispersive spectroscopy (EDS) to analyze the chemical compounds that were formed on the surface of the electrode. For measuring the electrical resistance of nano-ink estimate, ohmmeter, XIOLE, XL830L, China, multi-meter employed. Falling ball viscometer (Anton Paar-AMVn, Germany) was utilized to measure the viscosity of nano-ink. In this study, cyclic voltammetry (CV) and electrochemical impedance spectroscopy (EIS) techniques were applied for determination of the behavior in different fabrication steps and also selectivity of the engineered immunosensor, where CV ($T_{equilibration}$: 0 s, E_{begin}: −1.0 V, $E_{vertex1}$: −1.0 V, $E_{vertex2}$: 1.0 V, E_{step}: 0.01 V, scan rate: 0.1 V s^{-1}), electrochemical impedance spectroscopy EIS ($T_{equilibration}$: 0 s, scan type: fixed, E_{dc}: 0.25 V, E_{ac}: 0.01 V, max-frequency: 100 000 Hz, min-frequency: 0.1 Hz). Square wave

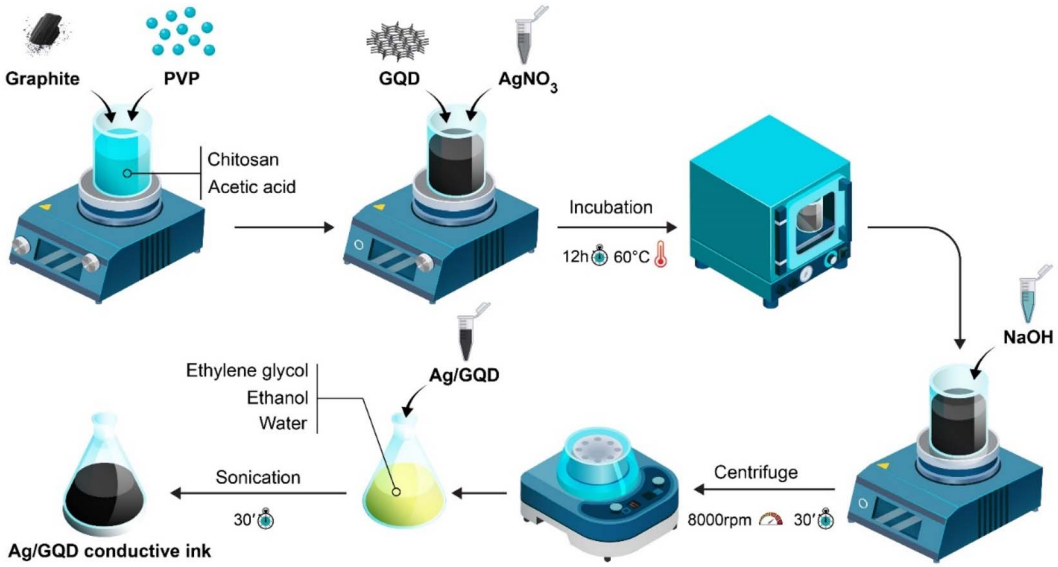

Scheme 1 Synthesis process of conductive AgNPrs–GQDs nano-ink.

voltammetry (SWV) and DPV applied for measuring reproducibility, repeatability and stability. The SWV technique data info ($T_{equilibration}$: 0 s, E_{begin}: −1.0 V, E_{end}: 1.0 V, E_{step}: 0.005 V, amplitude: 0.02 V, frequency: 10 Hz), and DPV technique data info ($T_{equilibration}$: 2 s, E_{begin}: −1.0 V, E_{end}: 1.0 V, E_{step}: 0.05 V, E_{pulse}: 0.1 V, T_{pulse}: 0.01 s, scan rate: 0.1 V s^{-1}). Chronoamperometry (ChA) method was used for analytical studies, ChA data info ($T_{equilibration}$: 2 s, E_{dc}: 0.3 V, t interval: 0.1 s, t run: 100 s).

3. Results and discussion

3.1. AgNPrs/GQD nano-ink conductivity analysis

In order to analysis of conductivity of nano-ink on the surface of paper, electrical conductivity was checked using an LED lamp, and also, an ohmmeter which was utilized to examine the resistance of nano-ink stabilized on the surface of a photographic paper. This was achieved by producing conductive tracks on the paper surface. The resulting measurement of resistance yielded a value of approximately 6.46 mΩ. To generate an electric current, it is essential to employ a battery holder of equivalent dimensions to the battery being utilized, to ensure proper integration of a battery within a circuit. After inserting the battery into the holder, the next step involves establishing electrical connections between the two wires emanating from the holder and the wire of the LED lamp source. The other unconnected wire of the LED was then connected to the designated surface coated with AgNPrs–GQD nano-ink, resulting in the illumination of the LED (Fig. S1 and S2) and video file.†

3.2. Characterization of synthesized nano-ink using TEM, XRD and Raman spectra

The TEM images (Fig. S1 (see ESI)†) of the bare AgNPrs were recorded and similar results were obtained according to previous reports.[23] It is found that, average particle sized is 10–50 nm. Also, bulk AgNPrs/GQDs nano-ink were recorded for extra confirmation, indicating proper ink synthesis (Fig. S1 (see ESI)†). It is noteworthy that the large-scale sheets are due to the presence of graphite, and silver nanoparticles are scattered on these sheets.

3.3. Fabrication of the immunosensor

Photographic paper was used as appropriate substrate to prepare the electrochemical biosensor. At first, photographic papers with dimensions of 2 × 3 centimeters were prepared. In the initial phase, paper-based electrodes (PBE) were fabricated by promptly applying conductive lines onto the surface of photographic paper using direct writing of nano-ink (AgNPs–GQDs). This application was achieved through the utilization of pen-on-paper technology, followed by a subsequent drying period at room temperature for a duration of 5 minutes (Scheme 2). It is important to point out that, the electrode is designed for one-time use or if it can be reused for multiple experiments. We use a Kapton polyimide film to minimize electrolyte absorption.

For activation of the –COOH groups of antibodies, 10 μl of biotinylated antibody was mixed with EDC/NHS and incubated for 20 min at 25 °C.

In pursuit of this objective, a mixture composed of EDC/NHS solution and biotinylated antibody was prepared in a 2 : 1 ratio. Next, a 5 μl of biotinylated antibody was immobilized on the surface of working electrode (central zone of three electrode template and incubated for 2 hours in room temperature). For deactivation of unreacted areas, 5 μl of BSA 10% solution was used and incubated for 30 minutes. Finally, 5 μl of standard LYVE-1 antigen was added, incubated for 2 hours (see Scheme 2 for more information). For the electrochemical evaluation of sensor performance, a 0.1 M solution of ferrocene in the presence of 0.1 M KCl was used. Also, first comparative electro-

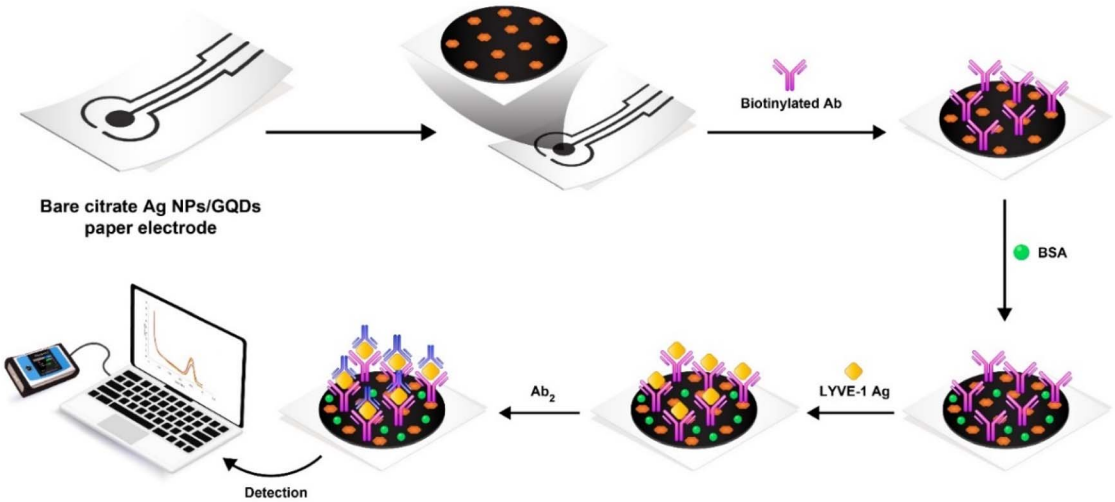

Scheme 2 Fabrication process of the immunosensor for the monitoring of LYVE-1.

analysis was done by CV and EIS techniques, which will be discussed on the next part of this report.

3.4. Characterization of different stages of the immunosensor's fabrication

3.4.1. FE-SEM study. FESEM images of the substrate (paper) modified by AgNPrs–GQD nano-ink, biotin-Ab–AgNPrs–GQD nano-ink, biotin-Ab–BSA–AgNPrs–GQD nano-ink, biotin-Ab–BSA–Ag–AgNPrs–GQD nano-ink, were recorded toward analysis of morphology and size of particles (Fig. 1 and S2 (see ESI)†).

As shown in Fig. S3 and S5 (see ESI),† the synthesized AgNPrs–GQD nano-ink composites were successfully stabilized on the surface of paper. In addition, the binding of the synthesized AgNPrs–GQD nanoink to Ab–BSA and the electrode surfaces was imaged by energy dispersion. According to the obtained results, the different arrangement of the nanoparticles can be clearly seen. Also, at the second step (immobilization of Ab on the AgNPrs–GQDs modified paper), the morphology of particles was generally changed and confirmed successful interaction (binding) of Ab to AgNPrs of conductive ink nanocomposite based on Ag–Ab bioaffinity. The final step is construction of Ab–Ag immunocomplex towards detection of biomarker. As can be seen, after interaction of biotinylated Ab with LYVE-1, the structure of working electrode interface was totally changed, which confirmed appropriate immobilization of antigen on the Ab–BSA–(AgNPrs–GQDs nano-ink). In summary, the FESEM technique has provided valuable images regarding the different steps of the immunosensor, using paper-based sensor strategy. All of these results were confirmed by EDS analysis (Fig. S4 (see ESI)†).

3.5. Electro-analytical study

Below, we describe the most important measurements of this study, which were performed as part of the development of an appropriate biosensor for immune-analysis.

3.5.1. Electrochemical behavior of immunosensor. The electrochemical immunosensor engagements the antibody as a capture agent and quantitatively processes the electrical signal subsequent from the binding event between the target molecule such as antigen as target molecule. In this study, electrochemical behavior of immunosensor was evaluated using CV and EIS techniques (Fig. 2).

As illustrated in Fig. 3, the electrochemical response of the immunosensor was examined at various stages of its assembly. Notably, there were distinct electrochemical characteristics observed between the bare electrode and the antibody-modified electrode. Subsequently, when the antibody–antibody (Ag–Ab) modified electrodes were introduced in the next step, they exhibited a different electrochemical profile. According to the obtained results, the highest current intensity is related to the paper-based electrodes modified with AgNPrs/GQD nano-ink (33.71 μA). Further, with the addition of antibody, the current intensity was decreased significantly (25.13 μA). Also, with the addition of the LYVE-1 Ag, the current intensity was decreased from 25.13 μA to 4.065 μA. In this way, the decreasing trend in flow intensity and peak height is clearly evident. These differences refer to Ab–Ag interaction with electrode surface and also, related to used nanomaterials and their affinity to Ab–Ag–electrode.

The diameter of the semicircle of the Nyquist plot represented 3007 Ω resistance, related to paper-based electrodes modified with AgNPrs/GQD nano-ink. The impedance has increased to 3290 Ω by adding Ab on the electrode modified with AgNPrs/GQD nano-ink. The semicircle of the Nyquist plot related to the AgNPrs/GQD nano-ink–Ab–BSA was started at 8800 Ω, but the semicircle of Nyquist plot of AgNPrs/GQD nano-ink–Ab–BSA–LYVE-1, was started at 9510 Ω.

According to the obtained results, the electroconductive layer of AgNPrs–GQD nano-ink on the surface of paper lead to high electrical conductivity and a large specific surface area, allowed more $(Fe(CN)_6)^{3-/4-}$ to reach its surface and electron transfer to occur at a higher rate. So, the prepared interface

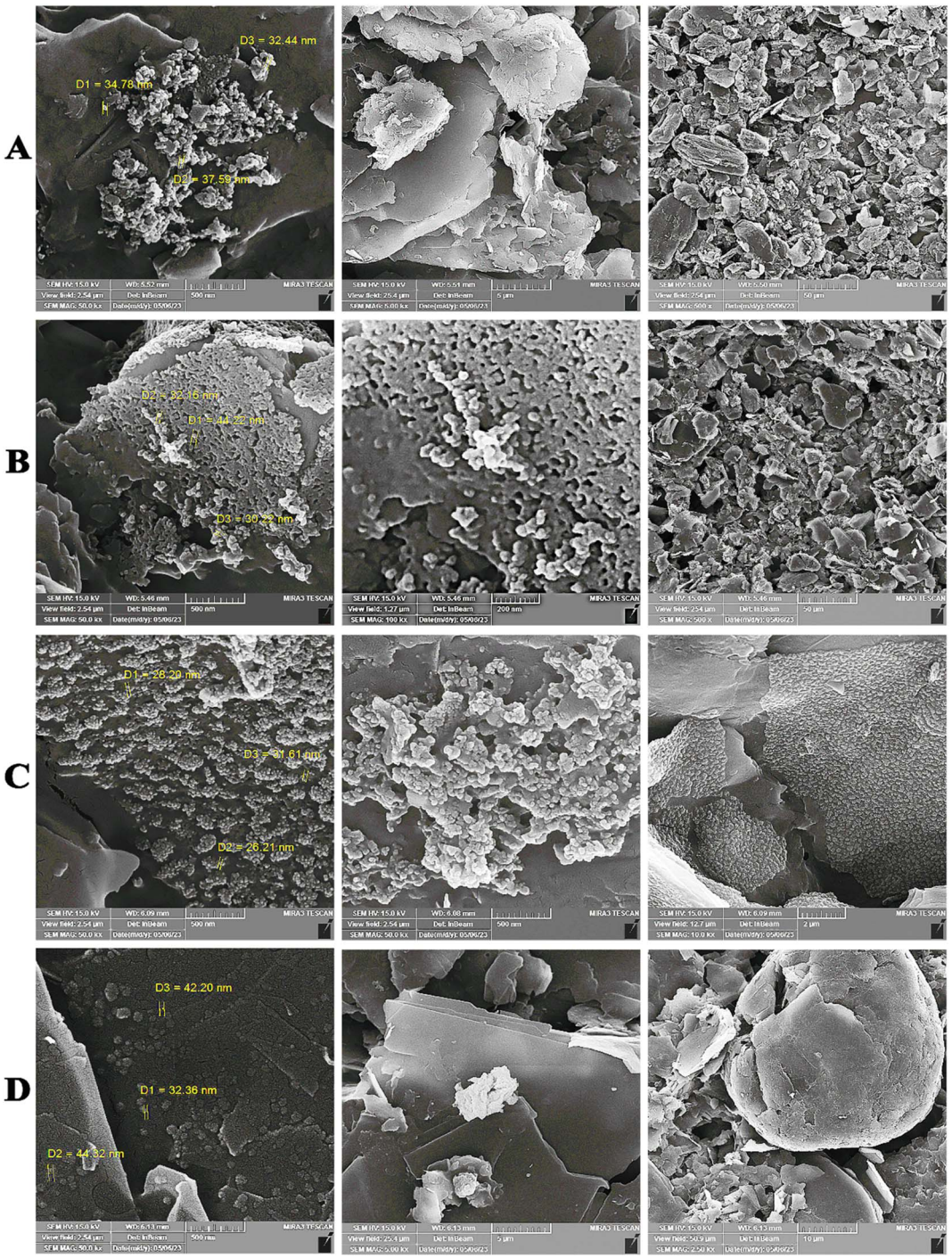

Fig. 1 FESEM images related to working electrode modified by (A) AgNPrs–GQDs nano-ink (B) AgNPrs–GQDs nano-ink–Ab, and (C) AgNPrs–GQDs nano-ink–Ab–BSA, (D) AgNPrs–GQDs nano-ink–Ab–BSA–Ag, with different magnifications to describe various levels of enlargement.

shows high electrocatalytically behavior for the electron transfer process of electrolyte towards high speed of redox process based on increased the rate of electron transfer and demonstrated appropriate electroactivity. Therefore, the AgNPrs–GQD are promising candidates for forming an antibody-active substrate. However, when the biotinylated antibody was assembled on the conductive ink-modified paper *via* the AgNPrs reaction, the peak currents of CV obviously decreased, which led to a decrease in the peak height. This result illustrated that as a biological species, antibody (bioreceptors) was successfully stabilized on the surface of AgNPrs–GQDs modified-paper. Because antibody as macromolecule occupy a large portion of the electrode surface, it inhibits redox process of Fe(III) to Fe(IV) which reduces the electron transfer of ferro/ferri (supporting electrolytes). So, antibody function as an insulator, slowing down electron transmission. Finally, in the presence of antigen

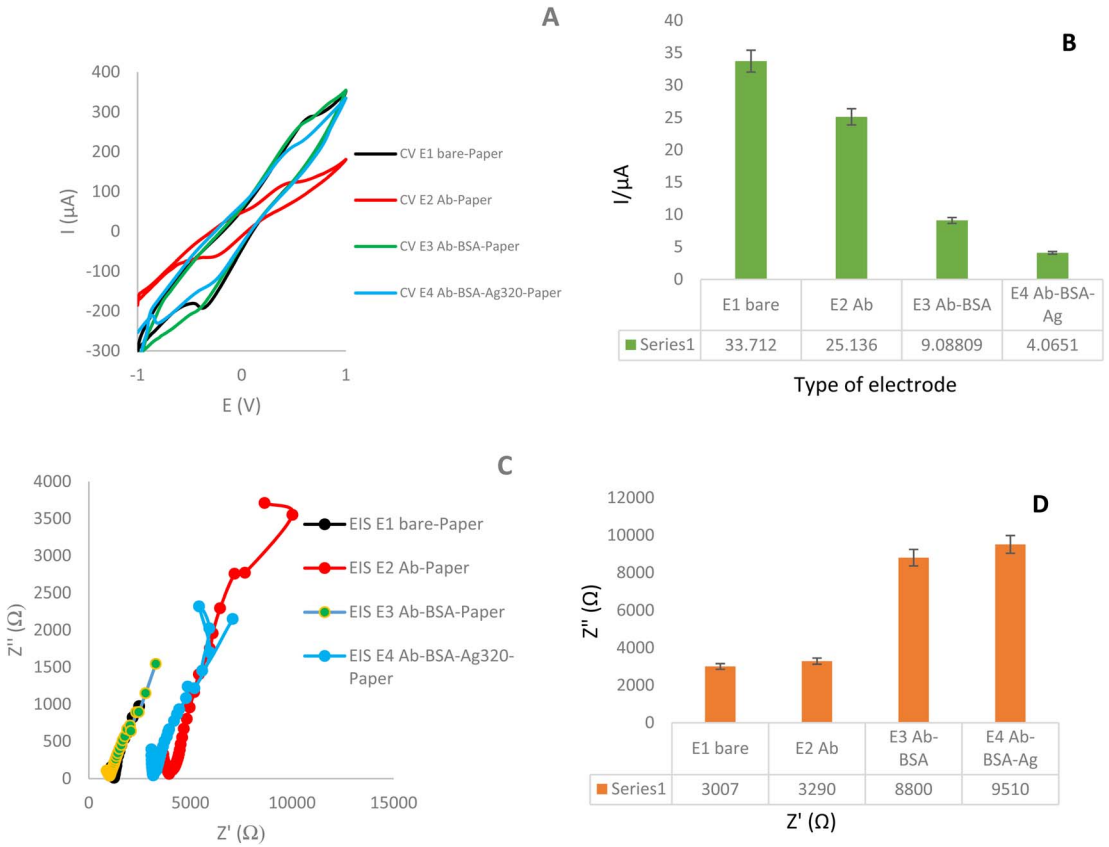

Fig. 2 (A and B) CVs and EIS of paper-based electrodes modified with AgNPrs/GQD nano-ink, AgNPrs/GQD nano-ink/biotin-Ab, AgNPrs/GQD nano-ink/biotin-Ab/BSA10%, AgNPrs/GQD nano-ink/biotin-Ab/BSA10%/LYVE-1 Ag. (C and D) Histograms of peak current *versus* types of modified paper-based electrodes. Supporting electrolyte was $K_4Fe(CN)_6/K_3Fe(CN)_6$/KCl (0.1 M).

(target), it was observed that the anodic peak current decrease again which point to the presence of analyte, as a result of the immune-complex on the surface of the electrode. So, the presence of analyte lead to hindrance of redox process Fe(III) to Fe(IV) based on low speed of electro-oxidation behavior mediator. All of these results were confirmed by EIS. So, it is clear that the designed immunosensor is capable of monitoring of antigen LYVE-1.

3.5.2. Sensitivity assessment. Sensitivity and specificity are important factors in biosensor development. High sensitivity is one of the main advantages of biosensors that specify biosensors performance from old methods.[56,57] Therefore, measurement of sensitivity and other analytical properties such as linear range is requested in biosensor performance validation. Accordingly, analytical properties were assessed by ChA technique (Fig. 3). Based on obtained results, there is two steps for the calibration curves. In the first step, immunosensor was applied for the determination of high concentration of LYVE-1 (20, 80 and 320 pg ml^{-1}) with regression equation of 0.99.

In the second step, the constructed immunosensor was applied for the measurement of low concentration of analyte which regression equation is 0.93. Using these results there are two linear range for this immunosensor. Also, low limit of quantification (LLOQ) was about 0.312 pg ml^{-1}. Experimental data obtained on 4 different electrodes (dots) and linear regression (line) are presented. Linear regression: I (μA) = 229.94 log $C_{(LYVE\text{-}1)}$ + 67.452, R^2 = 0.9346.

Several effective methods exist for determination of hyaluronic acid. However, these methods primarily depend on the hydrolysis of HA and come with various limitations, including discontinuity, strict detection conditions, and time-consuming procedures. In response to these challenges, certain researchers have explored alternative techniques involving various such as the turbidity assay,[58] ELISA,[59,60] colorimetry,[61] resonance Rayleigh scattering,[62] and lateral flow immunoassay,[63] fluorescence signals,[64] and high-performance liquid chromatography (HPLC).[65] As present in Table 1, there has not been a fully established methodology for the quantification of LYVE-1 or characterization of hyaluronan.

As it has been determined in the comparison of recent studies with the biosensor developed in this work, the most important feature and innovation of the current technique is the type of synthesized nanocomposite, low-cost, fast operation, mobility as well as good sensitivity and specificity. It seems that the appropriate sensitivity of the engineered system in this study is directly related to the synthesized nanocomposite.

3.5.3. Study of repeatability. A reliable LYVE-1 immunosensor should have excellent accuracy, reproducibility, and reproducibility.[28,66] The repeatability generated by the LYVE-1 immunosensor was considered by evaluating the anodic

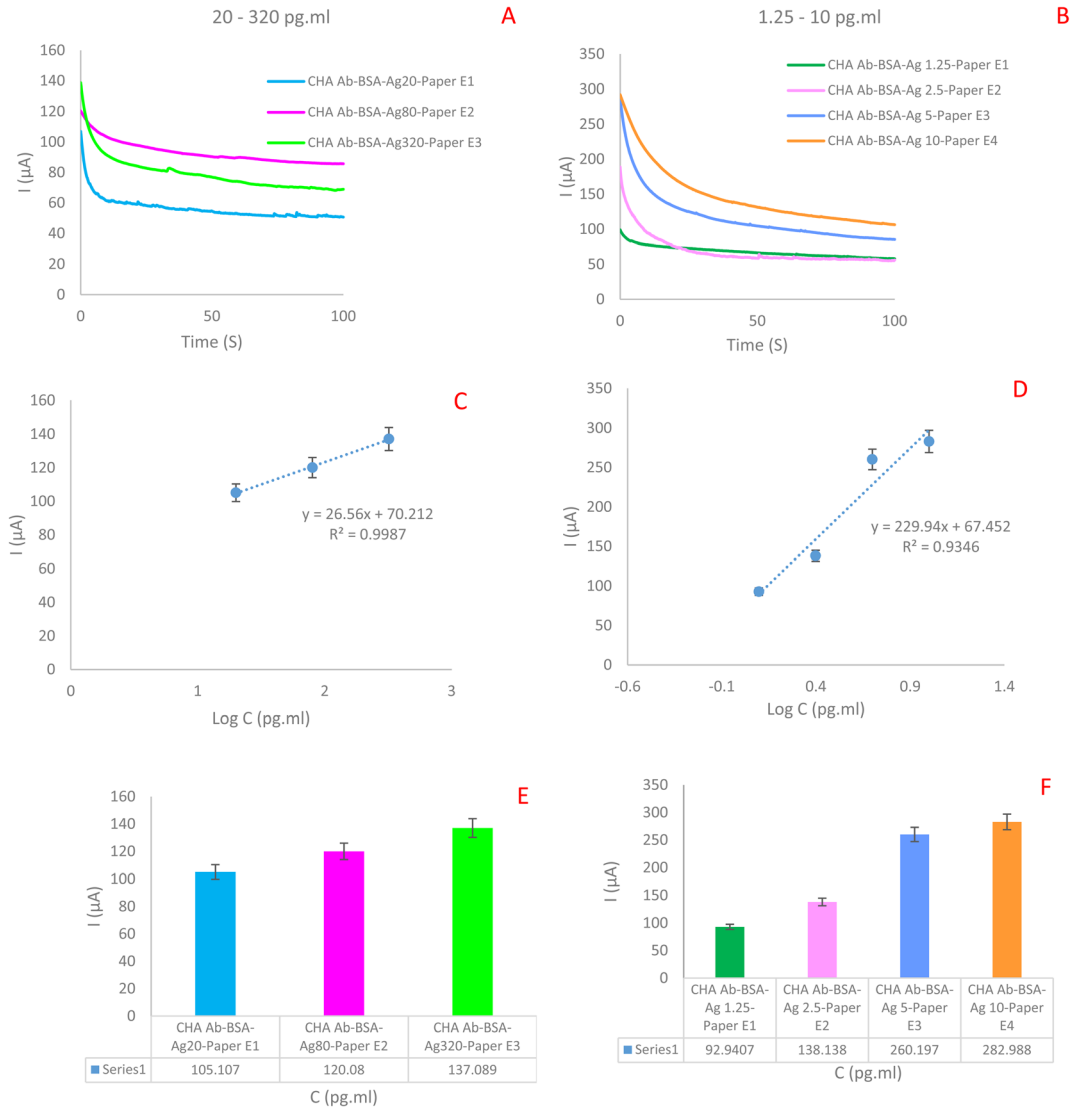

Fig. 3 (A and B) ChA of immunosensor in different concentrations of LYVE-1 Ag (1.25, 2.5, 5, 10, 20, 80 and 320 pg ml^{-1}). (C–F) Calibration curves of immunosensor in different forms (*I vs. C* and *I vs.* log *C*), respectively. Supporting electrolyte was 0.1 M $K_4Fe(CN)_6/K_3Fe(CN)_6$ containing 0.1 M KCl ($t = 100$ s, $E = 0.25$ V).

current generated by three types of same immunosensor prepared in the similar condition. Then DPVs of portable biosensor was recorded for three types of similar electrodes in the same condition. According to the obtained results, the average SD is 0.96 which is acceptable based on FDA guideline (Fig. S5 (see ESI)†).

3.5.4. Study of reproducibility. The reproducibility of the developed immunosensor was calculated by measuring the current generated *via* the anodic current generated by immunosensor in [AgNPrs–GQDs nano ink/biotin-Ab/BSA/Ag (20 pg ml^{-1}) (pH 6.0)] using three different biosensors. For the electrochemical evaluation, SWV technique was applied which is sensitive method for the reproducibility studies (Fig. S6 (see ESI)†). The signals obtained were calculated and standard deviation was reported. Using SWV technique acceptable reproducibility in the target measurements was achieved which indicated by their SD value. Using this immunosensor the SD values were 2.96 and 2.76. In the other words, the reproducibility of the assay was only through three repeated experiments on different electrodes which achieved a mean standard deviation (RSD) of 2.96%.

3.5.5. Study of inter-day repeatability. In this work, in addition, inter-day reproducibility and reproducibility were calculated appropriately. For this purpose, the DPV of immunosensor was recorded for three days and the same conditions for test. The SD values were obtained as 10.33, 6.04 and 7.38 respectively for three days' test, which confirmed inter-day repeatability of immunosensor for the monitoring of LYVE-1 (Fig. S7 (see ESI)†).

3.5.6. Cyclic stability of engineered surface. The stability of biosensors is often one of the deciding factors for the commercial viability of that particular device.[67] Used materials

Table 1 The methodologies devised for the determination of LYVE-1

Detection method	Sample	Detection time	Detection range	Limit of detection	Adv/disadv	Ref.
Turbidity assay	Cultured broth	NR	2.35 ± 0.04 mg ml^{-1}	NR	It is a fast process and does not harm bacteria/it does not distinguish between living and dead cells	58
ELISA	White rabbits' blood	NR	28 ± 17 ng ml^{-1}	NR	High specificity/sophisticated techniques and expensive culture media are required	59 and 60
Colorimetry	Complex samples	25–60 min	3–2000 mg l^{-1}	0.3 mg l^{-1}	Simple operation, quick response, adaptable sensitivity/fairly expensive, some surfaces reflect light, making it difficult to take measurements, cannot be used colorless compound	61
Resonance Rayleigh scattering	Eye drop	NR	0.4–48.0 μg ml^{-1}	0.096 μg ml^{-1}	Rapid analysis, high sensitivity and wide detection range/its stability is easily affected by the product	62
Lateral flow immunoassay	Carbohydrate-binding module (CBM) SrCBM70	5 min	NR	0.1 μg ml^{-1}	Simple, user-friendly operation difficult to miniaturize sample volume, high sensitivity and specificity multiplexing can be challenging, low sample volume required/unclear patent situation in some instances	63
Fluorescence signals	Human serum	Lower than 5 h	0.2 and 500.0 μg l^{-1}	0.2 μg l^{-1}	Superior image clarity over fluorescence microscopy/prolonged exposure to fluorescent light can result in bleaching and loss of fluorescence intensity	64
High-performance liquid chromatography (HPLC)	Pharmaceutical formulations	NR	320–480 μg ml^{-1}	NR	Complexity, expensive, time consuming	65
Paper-based immunosensor	Human plasma	NR	20–320 pg ml^{-1} and 0.625–10 pg ml^{-1}	0.312 pg ml^{-1}	Cost-effective, portable, fast, sensitive	This work

and their affinity and interactions with electrode surfaces are the most important factors that affect biosensor stability.[67,68] CVs technique was applied for the stability of the prepared interface on the surface of paper (substrate). As displayed, planned immunosensor showed satisfactory stability in different use (till 10th cycle) (Fig. S8 (see ESI)†).

3.5.7. Study of inter-day stability of surface. The long-term stability of the AgNPrs–GQD nano-ink modified photographic paper was evaluated using the SWV technique, as illustrated. The obtained results demonstrate that the current intensity on the initial day was recorded as 75.45 μA, which exhibited a slight decrease to 70.85 μA and 65.29 μA after 24 hours and 48 hours' incubation in dark condition, respectively. These changes in current intensity were not significant and is legible. Also, the standard deviation for the inter-day stability of the prepared substrate (paper–AgNPrs–GQD nano-ink) was determined as 0.078%, indicating suitable stability. The stability of the immunosensor was tested in three consecutive days and in completely identical conditions. The obtained results show acceptable stability. As can be seen in the recorded graphs, the current intensity has not changed significantly during three consecutive days and it is around 200 μA. It seems that the nanocomposite that used in the design of the biosensor had a good stability for 72 h (Fig. S9 (see ESI)†).

3.5.8. Study of selectivity. Selectivity characterizes the ability of an analytical technique to detect the target analyte without being influenced by other sample constituents.[69] It denotes one of the crucial advantages of biosensors, compared to other devices, as they allow to determine an analyte in a complex mixture without resorting to former separation.[69] For selectivity evaluating, CV technique was employed properly. In this part three different antigen (CA15-3, CEA and PSA) were used. As can be seen, recoded graph for LYVE-1 was entirely different from other used antigens. Based on signal-off strategy of designed immunosensor the obtained peak currents for LYVE-1, LYVE-1-PSA, LYVE-1-CEA and LYVE-1-CA15-3, were 12.06 μA, 99.99 μA, 158.73 μA and 77.34 μA, respectively. In the other words, planned immunosensor presented suitable selectivity and applicable for bioanalysis in the complex systems (Fig. S10 (see ESI)†).

3.5.9. Analytical study in human plasma samples (real sample analysis). The study of electrochemical behavior in the various concentration is the critical section in the biosensors engineering. So, application of immunosensor for the determination of LYVE-1 in different concentrations (0.625, 1.25, 5, 10, 20, 40, 160 and 320 pg ml^{-1}) spiked in human plasma samples (Fig. 4). Linear regression I (μA) = −142.16 log $C_{LYVE\text{-}1}$ + 255.98, R^2 = 0.9425. Based on ChA measurements, a pulse

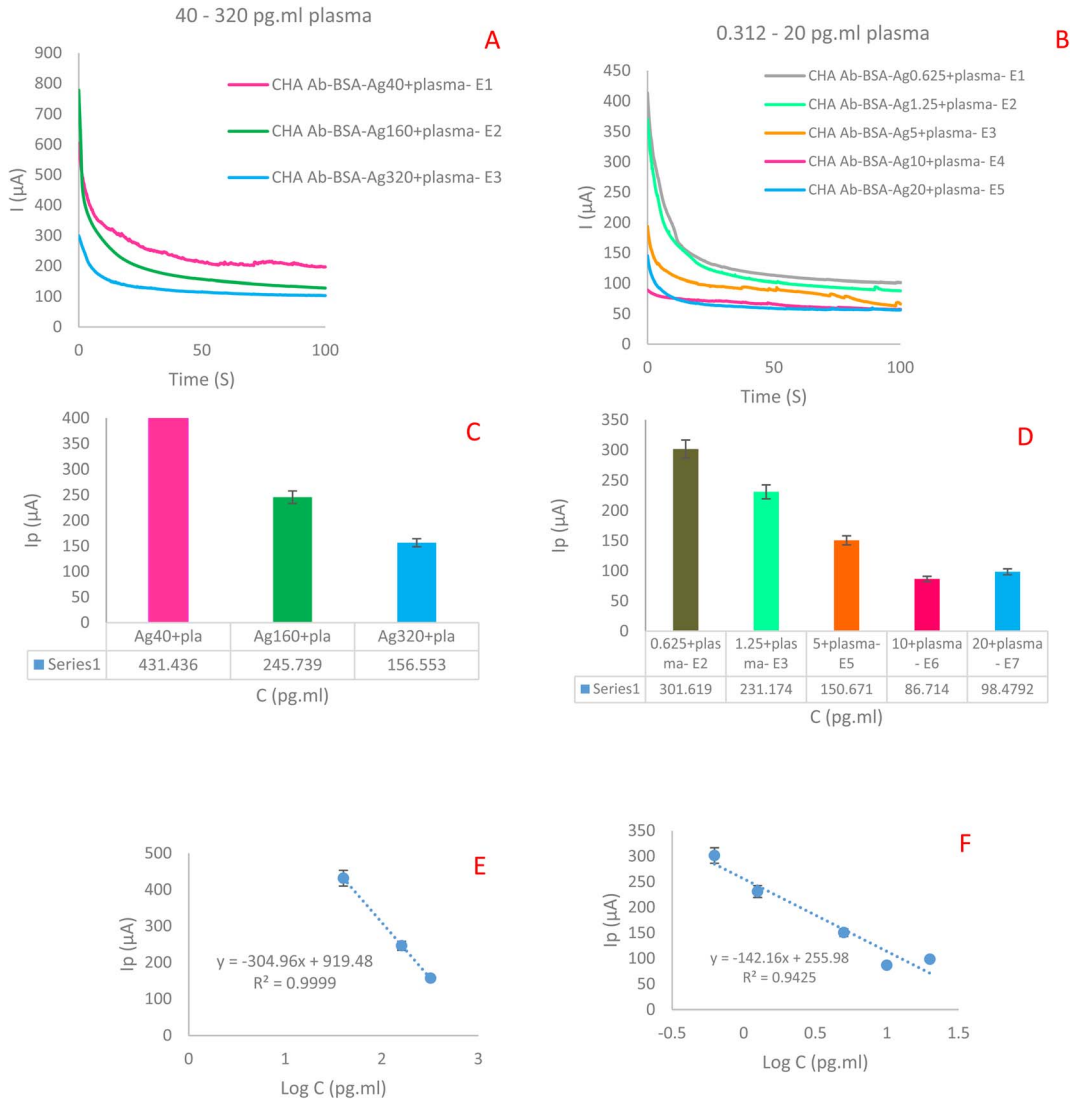

Fig. 4 (A and B) ChAs of immunosensor in plasma samples (0.625, 1.25, 5, 10, 20, 40, 160 and 320 pg ml^{-1}). (C–F) Calibration curves of immunosensor in different forms (*I vs. C* and *I vs.* log $C_{LYVE\text{-}1}$), respectively. Supporting electrolyte is 0.1 M $K_4Fe(CN)_6/K_3FE(CN)_6$ containing 0.1 M KCl.

height of 300 μA and a width of 300–800 μA were used along a step height of 0.25 V and a step time of $t = 100$ s.

4. Conclusion

The primary goal of this investigation was to provide a novel portable electrochemical biosensing platform for the quantitative detection of LYVE-1 in human plasma samples which was constructed based on AgNPrs and conductive nano-ink stabilized on the surface of paper using suitable three electrode template. Material applied for the quantitative determination of LYVE-1 plasma samples was effortlessly and cost-effective. The remarkable achievement of this study is the construction of a new immunosensor for the sensitive detection of the LYVE-1. The designed sensor showed good linear ranges of 20–320 pg ml^{-1} and 0.625–10 pg ml^{-1}, with the low detection limit (LOD) of 0.312 pg ml^{-1}. It is lower than that of most of the existing developed methods. Moreover, planned nanosensor showed excellent selectivity that promises its use in the monitoring of LYVE-1 in complex samples and assistance for biomarker-related disease screening which is necessary for early-stage diagnosis of cancer.

Abbreviations

LYVE-1	Lymphatic vessel endothelial hyaluronan receptor-1
LOD	Low detection limit
LLOQ	Lower limit of quantitation
QDs	Quantum dots
ssDNA	Single strand DNA
AgNPrs	Silver nanoprisms
ELISA	Enzyme-linked immunosorbent assay
CV	Cyclic voltammetry

SWV	Square wave voltammetry
DPV	Differential pulse voltammetry
PVP	Polyvinylpyrrolidone
TSC	Trisodiumcitrate
KCl	Potassium chloride
NHS	*N*-Hydroxysuccinimide
BSA	Bovine serum albumin
EDC	1-Ethyl-3-(3-dimethylaminopropyl)carbodiimide
FE-SEM	Field emission scanning electron microscope
EDS	Energy dispersive spectroscopy
XRD	X-ray diffraction
XPS	X-ray photoelectron spectroscopy

Conflicts of interest

The authors declare that they have no known competing financial interests or personal relationships that could have appeared to influence the work reported in this paper.

Acknowledgements

The authors would like to thank the Iran National Science Foundation (INSF) for funding this work, through a grant no. 99028845.

References

1 R. L. Siegel, K. D. Miller and A. Jemal, *Ca-Cancer J. Clin.*, 2018, **68**(1), 7–30.
2 N. Faraji, S. S. Arab, A. Doustmohammadi, N. L. Daly and A. Y. Khosroushahi, *Sci. Rep.*, 2022, **12**, 21341.
3 M. Morotti, A. Albukhari, A. Alsaadi, M. Artibani, J. D. Brenton, S. M. Curbishley, T. Dong, M. L. Dustin, Z. Hu and N. McGranahan, *Br. J. Cancer*, 2021, **124**, 1759–1776.
4 J. A. Rath and C. Arber, *Cells*, 2020, **9**, 1485.
5 S. Mardiana, B. J. Solomon, P. K. Darcy and P. A. Beavis, *Sci. Transl. Med.*, 2019, **11**(495), eaaw2293.
6 K.-Y. Huang, Y.-J. Tseng, H.-J. Kao, C.-H. Chen, H.-H. Yang and S.-L. Weng, *Sci. Rep.*, 2021, **11**, 13594.
7 F. Grisoni, C. S. Neuhaus, M. Hishinuma, G. Gabernet, J. A. Hiss, M. Kotera and G. Schneider, *J. Mol. Model.*, 2019, **25**, 1–10.
8 D. Jones, *Cells*, 2020, **9**, 762.
9 M. X. Luong, J. Tam, Q. Lin, J. Hagendoorn, K. J. Moore, T. P. Padera, B. Seed, D. Fukumura and R. Kucherlapati, *J. Cell. Physiol.*, 2009, **219**, 430–437.
10 V. Brezovakova and S. Jadhav, *J. Comp. Neurol.*, 2020, **528**, 2021–2032.
11 D. G. Jackson, *APMIS*, 2004, **112**, 526–538.
12 T. Wrobel, P. Dziegiel, G. Mazur, M. Zabel, K. Kuliczkowski and A. Szuba, *Lymphology*, 2005, **38**, 107–110.
13 C. M. Carreira, S. M. Nasser, E. di Tomaso, T. P. Padera, Y. Boucher, S. I. Tomarev and R. K. Jain, *Cancer Res.*, 2001, **61**, 8079–8084.
14 F. Ozmen, M. M. Ozmen, E. Ozdemir, M. Moran, S. Seçkin, D. Guc, E. Karaagaoglu and E. J. Kansu, *World J. Gastroenterol.*, 2011, **17**, 3220–3228.
15 M. Koukourakis, A. Giatromanolaki, E. Sivridis, C. Simopoulos, K. Gatter, A. Harris and D. J. Meinhardt, *Colorectal Cancer*, 2005, **58**, 202–206.
16 M. E. Karar, N. El-Fishawy and M. Radad, *J. Biol. Eng.*, 2023, **17**, 28.
17 C. Sethy, K. Goutam, B. Das, S. R. Dash and C. N. Kundu, *Vasc. Pharmacol.*, 2021, **140**, 106865.
18 R. Prevo, S. Banerji, D. J. Ferguson, S. Clasper and D. G. Jackson, *J. Biol. Chem.*, 2001, **276**, 19420–19430.
19 P. Ramani, J. V. Dungwa and M. T. May, *Virchows Arch.*, 2012, **460**, 183–191.
20 P. Bono, V.-M. Wasenius, P. i. Heikkilä, J. Lundin, D. G. Jackson and H. Joensuu, *Clin. Cancer Res.*, 2004, **10**, 7144–7149.
21 Y. Gao, Z. Liu, F. Gao and X.-y. Meng, *BMC Cancer*, 2010, **10**, 1–8.
22 K. Nunomiya, Y. Shibata, S. Abe, S. Inoue, A. Igarashi, K. Yamauchi, T. Kimura, Y. Aida, T. Nemoto and M. Sato, *J. Cancer*, 2014, **5**, 242.
23 A. S. Jauch, S. A. Wohlfeil, C. Weller, B. Dietsch, V. Häfele, A. Stojanovic, M. Kittel, H. Nolte, A. Cerwenka and M. Neumaier, *Cancer Cell Int.*, 2022, **22**, 1–17.
24 H. Y. Lim, S. Y. Lim, C. K. Tan, C. H. Thiam, C. C. Goh, D. Carbajo, S. H. S. Chew, P. See, S. Chakarov and X. N. Wang, *Immunity*, 2018, **49**(2), 326–341.
25 A. Fujimoto, Y. Ishikawa, Y. Akishima-Fukasawa, K. Ito, Y. Akasaka, S. Tamai, T. Maehara, H. Kiguchi, K. Ogata and C. Nishimura, *Am. J. Clin. Pathol.*, 2007, **127**, 82–88.
26 R. C. Fitzgerald, A. C. Antoniou, L. Fruk and N. Rosenfeld, *Nat. Med.*, 2022, **28**, 666–677.
27 S. Dolati, J. Soleymani, S. K. Shakouri and A. Mobed, *Clin. Chim. Acta*, 2021, **514**, 107–121.
28 A. Mobed, F. Kohansal, S. Dolati and M. Hasanzadeh, *RSC Adv.*, 2022, **12**, 28473–28488.
29 T. Mazzu-Nascimento, G. G. Morbioli, L. A. Milan, F. C. Donofrio, C. A. Mestriner and E. Carrilho, *Anal. Chim. Acta*, 2017, **950**, 156–161.
30 F. Bahavarnia, A. Saadati, S. Hassanpour, M. Hasanzadeh and A. Hassanzadeh, *Int. J. Biol. Macromol.*, 2019, **138**, 744–758.
31 X. Li, D. R. Ballerini and W. Shen, *Biomicrofluidics*, 2012, **6**(1), 11301–1130113.
32 F. Farshchi, A. Saadati and M. Hasanzadeh, *Heliyon*, 2020, **6**, e04327.
33 S. Hassanpour, M. Hasanzadeh, A. Saadati, N. Shadjou, J. Soleymani and A. Jouyban, *Microchem. J.*, 2019, **146**, 345–358.
34 F. A. Alatraktchi, J. S. Noori, G. P. Tanev, J. Mortensen, M. Dimaki, H. K. Johansen, J. Madsen, S. Molin and W. E. Svendsen, *PLoS One*, 2018, **13**, e0194157.
35 S. Hassanpour, M. Hasanzadeh, A. Saadati, N. Shadjou, J. Soleymani and A. Jouyban, *Microchem. J.*, 2019, **146**, 345–358.
36 J. Rajendran, *J. Hazard. Mater.*, 2023, **449**, 130979.

37 Y. Niu, Y. Han, H. Cheng, Z. Xiong, B. Luo, T. Ma, L. Li, S. Liu, X. Chen and C. Yi, *J. Mater. Res. Technol.*, 2023, **25**, 873–886.
38 Z. Duan, Z. Yuan, Y. Jiang, L. Yuan and H. Tai, *J. Mater. Chem. C*, 2023, **11**, 5585.
39 F. Farshchi, A. Saadati, N. Fathi, M. Hasanzadeh and M. Samiei, *Anal. Methods*, 2021, **13**, 1286–1294.
40 H. K. Kordasht, A. Saadati and M. Hasanzadeh, *Food Chem.*, 2022, **373**, 131411.
41 G. Jie, Q. Zhou and G. Jie, *Talanta*, 2019, **194**, 658–663.
42 Y. Yan, J. Gong, J. Chen, Z. Zeng, W. Huang, K. Pu, J. Liu and P. Chen, *Adv. Mater.*, 2019, **31**, 1808283.
43 M. Ozhukil Valappil, V. Pillai and S. Alwarappan, *Mater. Today*, 2017, **9**, 350–371.
44 P. Tian, L. Tang, K. Teng and S. Lau, *Mater. Today Chem.*, 2018, **10**, 221–258.
45 M. Li, T. Chen, J. J. Gooding and J. Liu, *ACS Sens.*, 2019, **4**, 1732–1748.
46 C. A. Ballesteros, L. A. Mercante, A. D. Alvarenga, M. H. Facure, R. Schneider and D. S. Correa, *Mater. Chem. Front.*, 2021, **5**, 7419–7451.
47 F. M. Winnik and D. Maysinger, *Acc. Chem. Res.*, 2013, **46**, 672–680.
48 Y. Wang, R. Hu, G. Lin, I. Roy and K.-T. Yong, *ACS Appl. Mater. Interfaces*, 2013, **5**, 2786–2799.
49 M. Jafari, M. Hasanzadeh, E. Solhi, S. Hassanpour, N. Shadjou, A. Mokhtarzadeh, A. Jouyban and S. Mahboob, *Int. J. Biol. Macromol.*, 2019, **126**, 1255–1265.
50 L. Xu, G. Yang, H. Jing, J. Wei and Y. Han, *Nanotechnology*, 2014, **25**, 055201.
51 Q. Lu, W. Wei, Z. Zhou, Z. Zhou, Y. Zhang and S. Liu, *Analyst*, 2014, **139**, 2404–2410.
52 L. Ruiyi, J. Yuanyuan, Z. Xiaoyan, L. Zaijun, G. Zhiguo, W. Guangli and L. Junkang, *Electrochim. Acta*, 2015, **178**, 303–311.
53 K. Lijuan, Y. Yongqiang, L. Ruiyi and L. Zaijun, *Electrochim. Acta*, 2016, **198**, 144–155.
54 X. Tan, Y. Li, X. Li, S. Zhou, L. Fan and S. Yang, *Chem. Commun.*, 2015, **51**, 2544–2546.
55 Q. Lu, Y. Zhang and S. Liu, *J. Mater. Chem. A*, 2015, **3**, 8552–8558.
56 Z. Fattahi, A. Y. Khosroushahi and M. Hasanzadeh, *Biomed. Pharmacother.*, 2020, **132**, 110850.
57 H. K. Kordasht and M. Hasanzadeh, *Anal. Methods*, 2020, **12**, 2795–2811.
58 J.-M. Song, J.-H. Im, J.-H. Kang and D.-J. Kang, *Carbohydr. Polym.*, 2009, **78**, 633–634.
59 P. Kongtawelert and P. Ghosh, *Anal. Biochem.*, 1989, **178**, 367–372.
60 R. S. Yahya, A. A. El-Bindary, H. A. El-Mezayen, H. M. Abdelmasseh and M. A. Eissa, *Clin. Lab.*, 2014, **60**, 1115–1121.
61 S. Pepeliaev, R. Hrudíková, J. Jílková, J. Pavlík, D. Smirnou, Z. Černý and L. Franke, *Eur. Polym. J.*, 2017, **94**, 460–470.
62 H. Q. Luo, N. B. Li and S. P. Liu, *Biosens. Bioelectron.*, 2006, **21**, 1186–1194.
63 X. Mei, M. Sun, Y. Zhang, J. Shen, J. Li, C. Xue and Y. Chang, *Int. J. Biol. Macromol.*, 2022, **223**, 1180–1185.
64 J. R. Martins, C. C. Passerotti, R. M. Maciel, L. O. Sampaio, C. P. Dietrich and H. B. Nader, *Anal. Biochem.*, 2003, **319**, 65–72.
65 K. Ruckmani, S. Z. Shaikh, P. Khalil, M. Muneera and O. Thusleem, *J. Pharm. Anal.*, 2013, **3**, 324–329.
66 F. Kohansal, A. Mobed, N. Aletaha, K. Ghaseminasab, S. Dolati and M. Hasanzadeh, *Microchem. J.*, 2023, **190**, 108649.
67 M. Song, X. Lin, Z. Peng, S. Xu, L. Jin, X. Zheng and H. Luo, *Front. Mater.*, 2021, **7**, 583739.
68 D.-W. Hwang, S. Lee, M. Seo and T. D. Chung, *Anal. Chim. Acta*, 2018, **1033**, 1–34.
69 B. Bucur, C. Purcarea, S. Andreescu and A. Vasilescu, *Sensors*, 2021, **21**, 3038.